Selective Gas Transport Through Few-Layered Graphene and Graphene Oxide Membranes

Hyo Won Kim,[1]* Hee Wook Yoon,[1]* Seon-Mi Yoon,[2,3]* Byung Min Yoo,[1] Byung Kook Ahn,[1] Young Hoon Cho,[1] Hye Jin Shin,[1] Hoichang Yang,[4] Ungyu Paik,[1] Soongeun Kwon,[5] Jae-Young Choi,[2,3]† Ho Bum Park[1]†

Graphene is a distinct two-dimensional material that offers a wide range of opportunities for membrane applications because of ultimate thinness, flexibility, chemical stability, and mechanical strength. We demonstrate that few- and several-layered graphene and graphene oxide (GO) sheets can be engineered to exhibit the desired gas separation characteristics. Selective gas diffusion can be achieved by controlling gas flow channels and pores via different stacking methods. For layered (3- to 10-nanometer) GO membranes, tunable gas transport behavior was strongly dependent on the degree of interlocking within the GO stacking structure. High carbon dioxide/nitrogen selectivity was achieved by well-interlocked GO membranes in high relative humidity, which is most suitable for postcombustion carbon dioxide capture processes, including a humidified feed stream.

Compared with traditional systems, membrane-based gas separations have allowed much simpler, more efficient separations (*1*). One of the challenges of developing membrane materials is to achieve high flux as well as high selectivity. Because a membrane flux is inversely proportional to the thickness of selective layer (from tens of nanometers to several micrometers), a graphene sheet with one-atom thickness has been considered as the ultimate membrane platform. In its defect-free form, however, graphene exhibits perfect barrier properties to all molecules and ions (*2*, *3*). Synthesis of large-area monolayer graphene by chemical vapor deposition (CVD) has recently been reported (*4*), and the resultant high-quality and uniform graphene sheet can be transferred to various substrates. We hypothesized that deposition of defect-free graphene sheets on gas-permeable polymer films would allow for preparation of flexible plastic barrier films to prevent gas and water vapor penetration. Therefore, we prepared polymer-supported thin films of graphene with varying numbers of deposited graphene sheets (Fig. 1A). Poly(1-methylsilyl-1-propyne) (PTMSP) was selected as the substrate because it is one of the most permeable, rigid, and glassy polymers available (*5*). The gas permeability of the resultant barrier films decreased as the number of graphene layers deposited increased. However, a single graphene-layered PTMSP film (G1/PTMSP) showed a relatively small reduction in gas permeability compared with the original PTMSP (Fig. 1B), implying the presence of defects generated during the CVD growth and transfer process (Fig. 1C). These defects also resulted in a large electrical sheet resistance (>2500 ohms per square) (Fig. 1B), similar to values reported in the literature (*6*). This sheet resistance was considerably reduced (<1000 ohms per square) as more graphene layers were stacked. The reduction in sheet resistance correlated well with the gas permeability of the film (Fig. 1B).

We anticipated that the porosity caused by the graphene sheet defects could be mitigated by depositing more graphene layers. Although the gas permeability of the films decreased gradually with increasing number of graphene layers, we were not able to obtain excellent barrier films. Surprisingly, the O_2/N_2 selectivity of G#/PTMSP films (where # represents the number of graphene layers) improved (Fig. 1D) with increasing graphene stacking, which suggests that gases diffused not only through defective pores on the graphene sheet but also between the graphene interlayers (*7*–*9*), leading to higher selectivity than the original PTMSP film. The O_2/N_2 selectivity increased from 1.5 (for PTMSP) to 6 (for G5/PTMSP), whereas the O_2 permeability decreased from 730 to 29 barrer [1 barrer = 1×10^{-10} cm^3 $cm/cm^2 \cdot sec \cdot cmHg$ at standard temperature and pressure (STP)], surpassing the O_2/N_2 separation limitation of polymeric membranes (*10*) with a selectivity similar to that of carbon molecular sieve (CMS) membranes (*11*).

A possible explanation for this phenomenon is that the defective graphene sheets were irregularly aligned, resulting in the formation of gas-permeable, slit-like interlayer spacings. Pristine graphene synthesized via CVD has a polycrystalline structure with grain boundaries linked to pentagon-heptagon pairs (*12*). Mechanical cleavage or oxidation at these sites can lead to sheet defects, such as tears or holes (*12*, *13*), which allow ingress of gas molecules. Furthermore, because of the irregular stacking caused by corrugations, wrinkles, and ripples, randomly stacked graphene sheets had an interplanar spacing larger than that of closely packed graphitic layers (0.335 nm). The average interlayer spacing of randomly stacked graphene layers on a silicon wafer was 0.355 nm, albeit with a broad spacing distribution, as measured by two-dimensional (2D) grazing-incidence x-ray diffraction (fig. S1). The interlayer spacing of the graphene layers on PTMSP would be larger because the surface of this polymer film is not as flat as that of mica or silicon wafers (*14*). The increase in selectivity of the G#/PTMSP films, with the number of graphene layers deposited, indicates the formation of slit-like interlayer spacings of similar size to those present in CMS membranes.

We investigated the gas permeation behavior of thin graphene oxide (GO) membranes. GO's interlayer spacing is larger than that for graphene—namely, 0.6 to 1.0 nm—depending on the preparation method and the presence of water intercalated in the GO layers (*15*, *16*). Thick (>10-nm) GO paper and thin (3- to 7-nm) GO membranes can be easily prepared by various solution methods, such as vacuum filtration, direct evaporation, and spray and spin coatings (*16*).

GO films in the dry state are not permeable to small gases (e.g., He), but water molecules permeate through hydrated GO films faster than expected (*17*). The potential energy barrier for gas entrance, tortuosity determined by the GO sheet size and thickness, layer structure, residual water content, and deformation of thin-layered structures during dewetting can all affect molecular transport in GO films. In contrast to graphene sheets, GO is not completely 2D (*18*), which suggests that GO should stack nonuniformly. For the above reasons, thin GO membranes should be permeable to small gases if sufficient transmembrane pressure is applied to overcome the energy barriers to pore entry and diffusion within pores or channels. In fact, we found that gas can permeate through even thick GO membranes at elevated transmembrane pressures and that the gas permeability can be tuned by changing the average GO sheet size (fig. S2). Furthermore, detectable gas permeance through the ultrathin GO membranes is strongly dependent on applied transmembrane pressure for a given average GO sheet size (fig. S3).

We used two different coating methods to prepare GO membranes on microporous polymeric membranes. The microporous polymeric support was selected to optimize both surface roughness and wettability to achieve a homogeneous coating. Among the commercially available supports, polyethersulfone (PES) membranes

[1]Department of Energy Engineering, Hanyang University, Seoul 133-791, Republic of Korea. [2]Samsung Advanced Institute of Technology (SAIT), Samsung Electronics, Suwon 446-712, Republic of Korea. [3]Graphene Research Center at SAIT, Suwon 446-712, Republic of Korea. [4]Department of Advanced Fiber Engineering, Inha University, Incheon 402-751, Republic of Korea. [5]Samsung Corning Precision Materials, Ansan 336-725, Republic of Korea.

*These authors contributed equally to this work.
†Corresponding author. E-mail: jaeyoung88.choi@samsung.com (J.-Y.C.); badtzhb@hanyang.ac.kr (H.B.P.)

yielded the most uniform coating (fig. S4). We prepared several-layer GO membranes by contacting the support membrane surface to the air-liquid interface of a GO solution, followed by spin-coating (method one). We also prepared thin GO membranes by spin-casting of a GO solution on the membrane surface (method two) (fig. S5). Macroscopically, after several coatings, both membrane surfaces appeared to be homogeneously coated by a GO thin film without detectable pinholes or cracks under an optical microscope. The color of the GO-coated membranes (light yellow) differed from that of the pristine PES membrane surface (white) (fig. S6). Transmission electron microscopy (TEM) revealed that the coated GO thicknesses were ~3 to 7 nm (Fig. 2, A and B), depending on the number of coating iterations. We selected these GO coating methods to test the relative importance of electrostatic repulsion and immersion capillary force on the GO stacking structure. When considering GO deposition by method one, initial GO solution-membrane contact is performed without spin casting so that GO deposition is governed by electrostatic and hydrophilic interactions between the GO sheets and the polymer membrane. Generally, in an alkaline aqueous solution, GO sheet edges are negatively charged due to pendant ionized carboxylic acid groups. Therefore, GO sheet edge-to-edge interactions are repulsive, leading to an island-like assembly of GO sheets on the membrane surface. After this initial GO deposition on the membrane surface, water between deposited GO sheets and GO sheets in solution is removed through spin casting, allowing strong attractive capillary forces to further deposit GO sheets from solution. A second iteration of the dipping procedure in method one leads to further GO deposition through face-to-face attractive interactions (for instance, van der Waals interactions and hydrogen bonding) between the size-mismatched GO sheets (*19*). We found that this method leads to a relatively heterogeneous GO deposition (Fig. 2, C and E), in which the GO stacking structure resembles islands. In contrast, method two, in which the GO solution-membrane contact occurs only during spin casting, leads to a considerably more dense GO deposition. Presumably, this dense stacking occurs because the face-to-face attractive capillary forces created by the spin coating overcome the repulsive edge-to-edge GO sheet interaction. Therefore, the initial deposition is governed more by capillary interactions between the GO sheet faces and not the electrostatic interaction between the GO edges (Fig. 2, D and F). Cross-sectional TEM images show different stacking structures using each coating method (Fig. 2, A and B).

Gas permeance [in gas permeation units (GPUs), 1 GPU = 1×10^{-6} $cm^3/cm^2 \cdot sec \cdot cmHg$ at STP] was measured at a feed pressure of 1 bar, using the common constant-pressure, variable-volume method. We found that the gas transport behavior of membranes prepared by methods one and two was very different. The GO membranes prepared by method one showed typical gas permeation behavior explained by Knudsen transport of gases in nanoporous membranes (Fig. 3A). Here, gas transport is determined by the pore size of the membrane and the free path length of the molecules in a gas mixture, and Knudsen diffusion leads to separation of gases with large differences in their molecular weights (*20*). As expected, gas permeance decreased according to the molecular weight of the gases. The selectivity of membranes prepared by method one to He was in good agreement with theoretical Knudsen selectivity, but this did not hold true for their selectivity to CO_2 (Fig. 3A). During the permeation test at a feed pressure of 1 bar, CO_2 permeance decreased sharply with time and stabilized after 1 hour, whereas other gases did not show this reduction (Fig. 3B). Consequently, the small gas/CO_2 selectivity of the membranes exceeded the Knudsen selectivity to a large extent; for example, the H_2/CO_2 selectivity was as high as 30, whereas the theoretical Knudsen selectivity of H_2/CO_2 is 4.67.

We now consider the role of both the porosity and chemical nature of the gas transport channels within the stacked GO structure. Highly interlocked, close-packed layering structures were not obtained, even after repeated coatings (fig. S7); rather, nanopores created by the edges of noninterlocked GO sheets formed within the GO structure. Gas permeation occurred through these nanopores, as confirmed by the Knudsen transport behavior of the GO membranes. Furthermore, a number of carboxylic acid groups line the pore outer walls, because free carboxylic acid groups are distributed at GO edges. Torrisi *et al.* calculated the isoteric heats of sorption for CO_2 in functionalized metal-organic frameworks and predicted that the incorporation of a carboxylic acid group would lead to the highest isoteric heat (*21*). Although CO_2 is a nonpolar gas, the polarity of the individual C-O bonds in the molecule allows for interaction with polar groups in GO. Thus, CO_2 can act as a Lewis acid or a Lewis base and can participate in hydrogen bonding. Carboxylic acid groups provide a preferential site for CO_2 adsorption, consequently retarding CO_2 transport in the nanopores by strongly trapping CO_2 molecules. This phenomenon is counterintuitive, because strong affinity between penetrant and nanopore walls often leads to surface diffusion of the penetrant preferentially sorbed on the pore wall, resulting in flux enhancement of highly sorbed or condensable penetrants (*22*).

Because GO is hydrophilic, we also evaluated the gas transport behavior of GO membranes

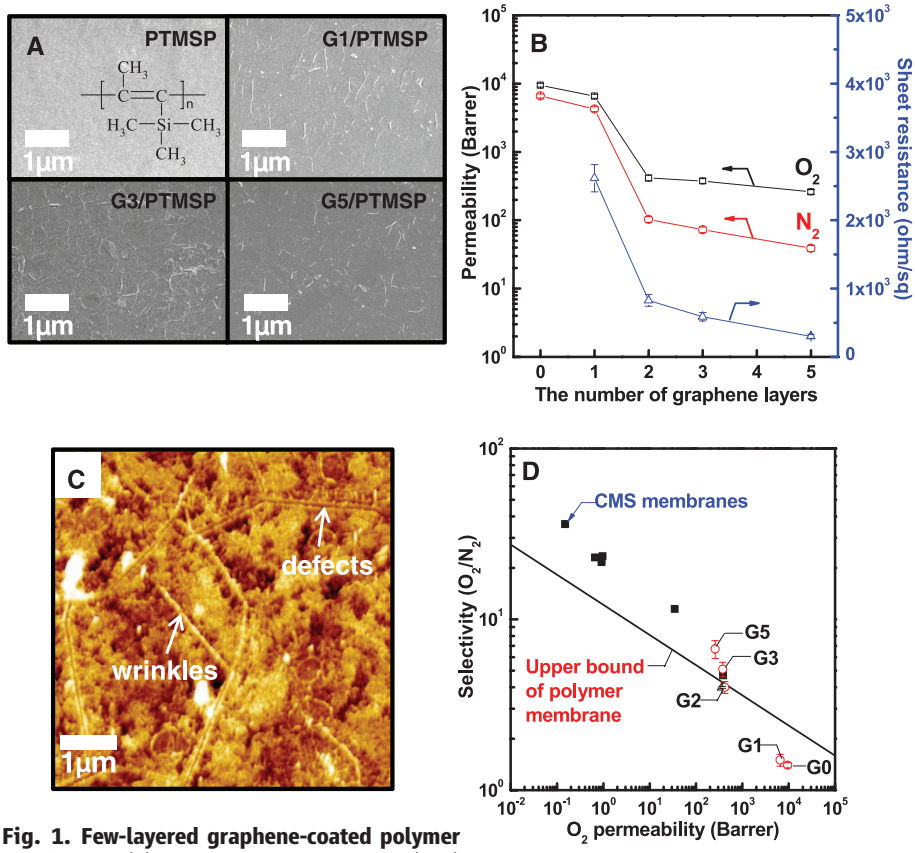

Fig. 1. Few-layered graphene-coated polymer membranes. (A) Scanning electron microscopy (SEM) images of graphene/PTMSP membrane surfaces. **(B)** Changes in gas permeability and sheet resistance of graphene/PTMSP membranes as a function of the number of graphene layers. Error bars indicate the SD of all raw data. **(C)** Atomic force microscopy (AFM) images of a graphene/PTMSP membrane surface. **(D)** Relation between O_2 permeability and O_2/N_2 selectivity of graphene/PTMSP membranes. The upper bound is from (*10*), as well as gas separation performance data of CMS membranes reported in the literature (*11*). Error bars indicate the SD in the current measured from five parallel experiments.

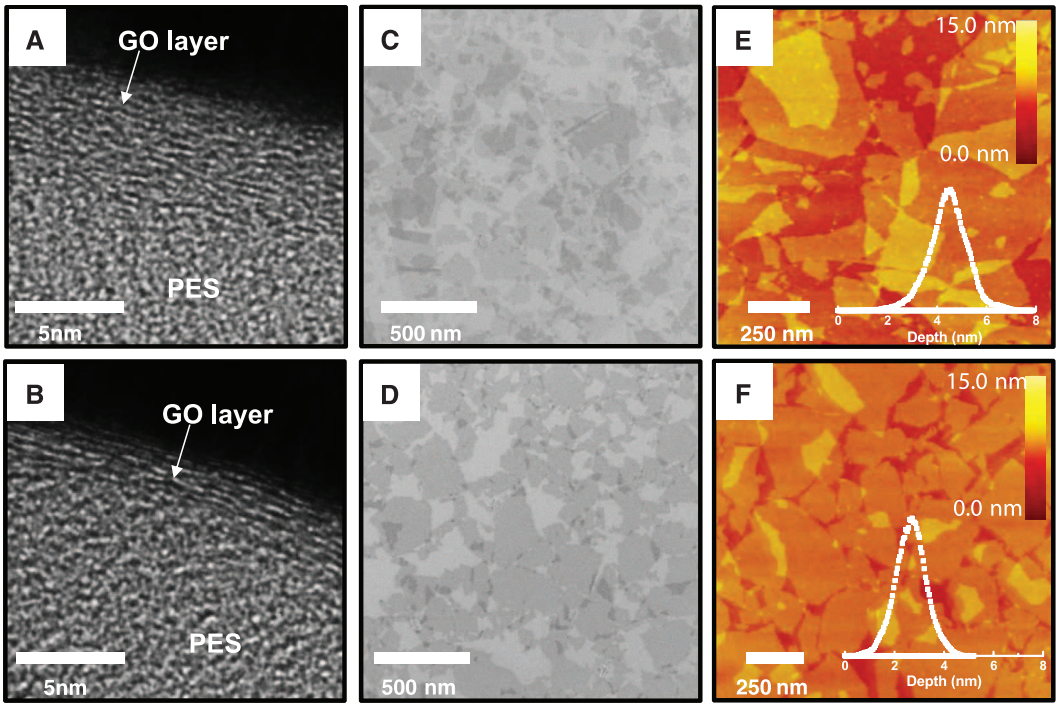

Fig. 2. Ultrathin GO membranes. Cross-sectional TEM images of ultrathin GO membranes. (**A**) Method one; (**B**) method two. SEM images of GO films coated on an SiO_x wafer (here, x indicates the number of O atoms). (**C**) Method one; (**D**) method two. AFM images of GO membrane surfaces and inert figures showing depth profiles of GO membrane surfaces. (**E**) Method one [root mean square roughness (R_q) = 0.8 nm, average roughness (R_a) = 0.614 nm]; (**F**) method two (R_q = 0.608 nm, R_a = 0.467 nm).

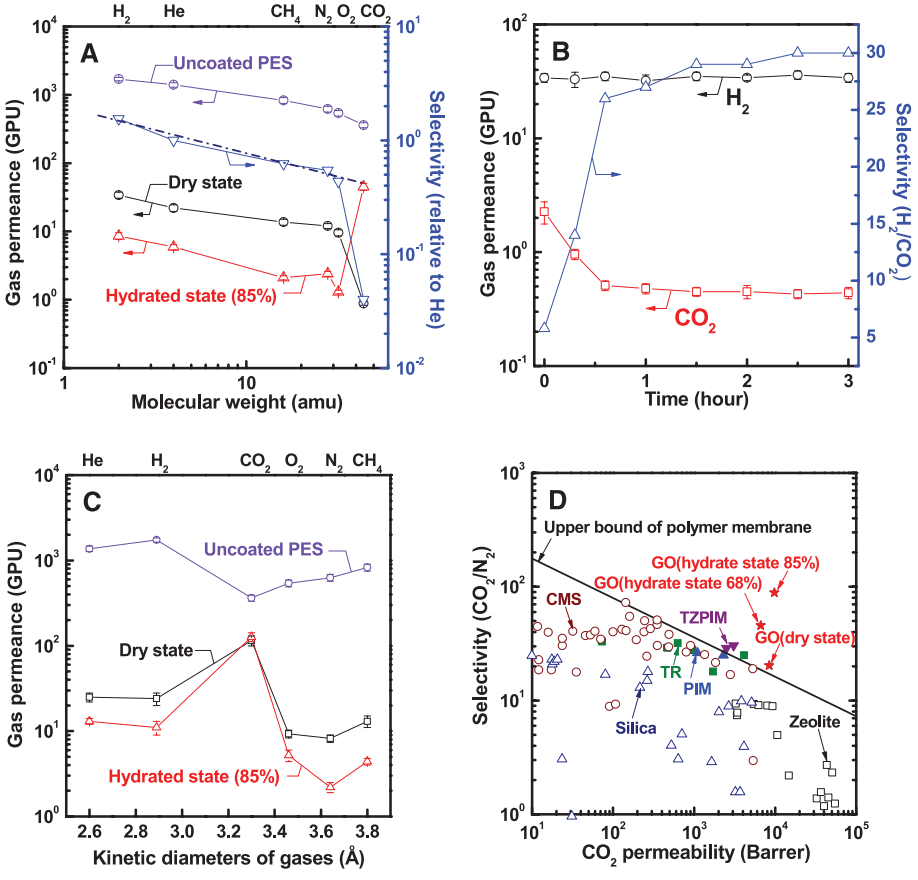

Fig. 3. Gas transport behavior through ultrathin GO membranes. (**A**) Gas permeances of GO membranes as a function of molecular weight (method one; dashed line represents the ideal Knudsen selectivity) under dry and humidified conditions. amu, atomic mass unit. (**B**) H_2 and CO_2 permeances and H_2/CO_2 selectivity of method one GO membranes as a function of permeation time. (**C**) Gas permeances of GO membranes as a function of kinetic diameter (method two) under dry and humidified conditions. (**D**) Relation between CO_2 permeability and CO_2/N_2 selectivity of method two GO membranes under dry and humidified conditions [TR (*23*); tetrazole PIM (TZPIM) and PIM (*25*); CMS (*26*)]. Error bars indicate the SD of all raw data.

(method one) by changing the relative humidity of the feed streams (Fig. 3A). In general, all gas permeances decreased as the humidity in the feed increased, implying that condensed water molecules in the pores or between layers hindered the transport of noncondensable small gas molecules. In contrast, CO_2 permeance was 50 times higher in the presence of water, leading to an enhancement in the selectivities of gas pairs of interest (for example, CO_2/CH_4, CO_2/H_2, and CO_2/N_2) (fig. S8).

GO membranes prepared by method two formed highly interlocked layer structures and also exhibited extraordinary gas permeation behavior, albeit different than the behavior exhibited by membranes prepared via method one. For these GO membranes, the gas permeance order at 298 K was $CO_2 > H_2 \geq He > CH_4 > O_2 > N_2$ (Fig. 3C). This order has been observed for a few high free-volume microporous glassy polymers, such as PTMSP, that consist of a loosely packed network of polymer chains with continuous channels or pores for diffusion (*5*, *23*). The gas transport behavior of these GO membranes means that they comprised closed-packed, interlocked GO layered structures. These GO membranes were less gas permeable than those prepared by method one but were also more selective, indicating that gases diffused selectively between the GO interlayers and, thus, had a different effective diffusion pathway. Based on the resistance model (*24*), we calculated the intrinsic gas permeability of the thin GO membranes. The CO_2 permeability is ~8500 barrer, and CO_2/N_2 selectivity is ~20. The separation performance is higher than that reported for CO_2 for polymeric membranes, including thermally rearranged (TR) polymers (*23*), polymers of intrinsic microporosity

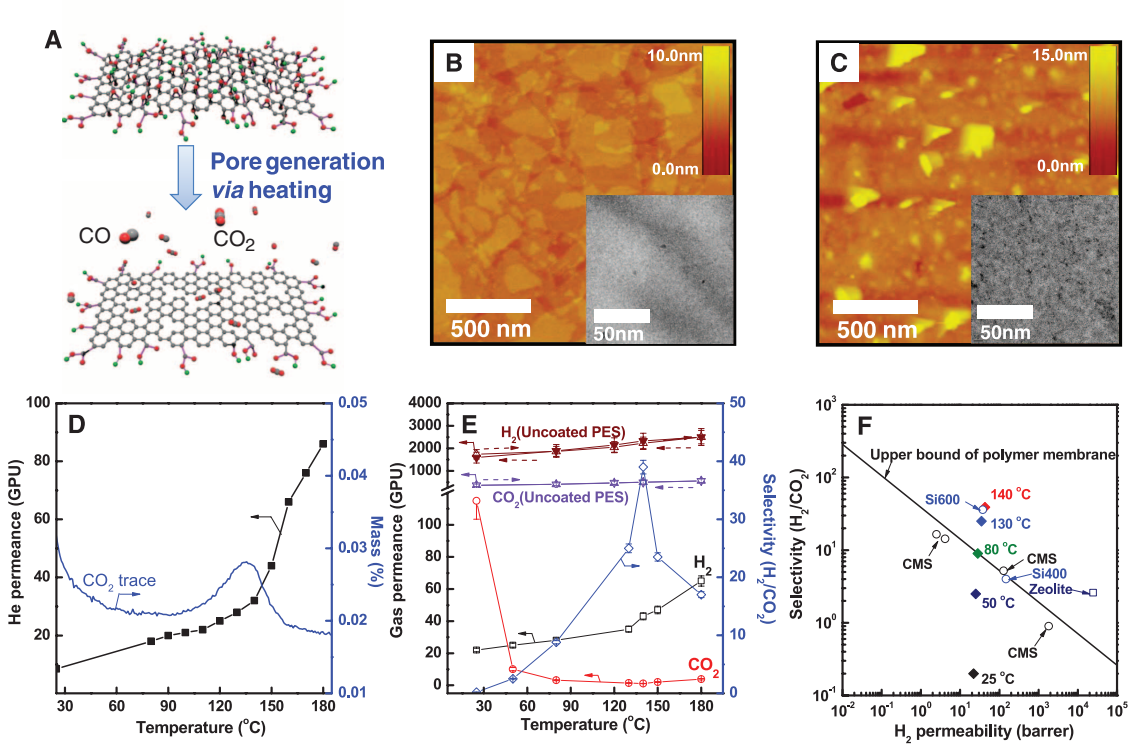

Fig. 4. Gas transport behavior through thermally reduced GO membranes. (**A**) Schematic illustration of pore generation in GO membranes using a thermal treatment process. AFM images of method two GO membranes (**B**) before (R_q = 0.553 nm, R_a = 0.450 nm) and (**C**) after thermal treatment at 180°C for 3 hours (R_q = 1.75 nm, R_a = 1.09 nm). The insets to (B) and (C), respectively, show TEM images before and after thermal treatment at 180°C for 3 hours. (**D**) He permeance trend and CO_2 trace of mass spectroscopy as a function of temperature. (**E**) H_2 and CO_2 permeability of thermally treated GO membranes as a function of temperature. Error bars indicate the SD of all raw data. (**F**) Comparison of gas separation performance between GO membranes and other membranes in the literature [polymers (*10*); CMS (*26*, *29*); zeolite (*26*); silica (*30*)].

(PIM) (*25*), and inorganic membranes, such as carbon, silica, and zeolite (*26*) (Fig. 3D). The gas permeances decreased gradually as the humidity increased (*27*), but the CO_2 permeance remained constant, irrespective of the relative humidity (fig. S9), resulting in highly CO_2-selective, ultrathin (<10-nm) carbon membranes (Fig. 3D and fig. S10).

More permeable, selective graphene-based membranes can be prepared by creating pores on the basal plane by simple heat treatment (Fig. 4, A to C). Thermal treatment of ultrathin GO membranes (prepared with method two) caused decomposition accompanied by the release of, primarily, water and CO_2 at a temperature of ~140°C, as confirmed by analysis with a thermogravimetric analyzer–mass spectrometer (Fig. 4D), consistent with the literature (*28*). At this temperature, CO and CO_2 are released from oxygen-containing functional groups on basal planes or at edges, resulting in irreversible defects. After the membrane was mounted in a cell surrounded by a heating chamber, the gas permeation rates of H_2 and CO_2 at a feed pressure of 1 bar were recorded as a function of cell temperature. Below 130°C, H_2 permeance increased gradually, whereas CO_2 permeance decreased steadily. At ~130° to 140°C, H_2 permeance increased abruptly and CO_2 permeance increased slightly (Fig. 4E), implying that thermal annealing made the microstructures of the GO active layers more porous due to irreversible pore formation. Without such structural deformation, the slope of gas permeance versus temperature should be linearly positive (for H_2) or negative (for CO_2) under thermally activated diffusion conditions. However, two distinct slopes were observed, presenting evidence of a more open porous structure. The gradual reduction in CO_2 permeance below 130°C is due to the low enthalpy of sorption. The increase in CO_2 permeance above 140°C also indicates more porous microstructures in the GO thin layers. The H_2/CO_2 permselectivity at 140°C was as high as 40 (Fig. 4F), which is one of the highest values reported for other comparable membranes (*10*, *26*, *29*, *30*).

Overall, transport in graphene or GO nanosheets has been covered less than that in carbon nanotubes, but there is great potential and the research area is growing. The ability to have adaptive and dynamic layer distances is a distinct attribute of stacked graphene or GO nanosheets. With careful control of the stacking structures, separation factors and flow rates can be further improved. Indeed, several layered GO membranes behave as either nanoporous (method one) or molecular-sieving membranes (method two) by the stacking method. Both membranes show CO_2-philic permeation behavior, which is further enhanced by the presence of water. As such, these membranes are promising materials for industrial CO_2 separation processes related to petrochemical engineering (CO_2 removal from natural gas), the environment (CO_2 capture from flue gas), and biomass energy (CO_2 recovery from landfill gas).

References and Notes

1. H. Strathmann, *Introduction to Membrane Science and Technology* (Wiley, Weinheim, Germany, 2011)
2. J. S. Bunch *et al.*, *Nano Lett.* **8**, 2458–2462 (2008).
3. O. Leenaerts, B. Partoens, F. M. Peeters, *Appl. Phys. Lett.* **93**, 193107 (2008).
4. X. Li *et al.*, *Science* **324**, 1312–1314 (2009).
5. T. Masuda, E. Isobe, T. Higashimura, K. Takada, *J. Am. Chem. Soc.* **105**, 7473–7474 (1983).
6. X. S. Li *et al.*, *Nano Lett.* **9**, 4359–4363 (2009).
7. D. E. Jiang, V. R. Cooper, S. Dai, *Nano Lett.* **9**, 4019–4024 (2009).
8. S. Blankenburg *et al.*, *Small* **6**, 2266–2271 (2010).
9. J. Schrier, *Am. Chem. Soc. Appl. Mater. Interfaces* **4**, 3745–3752 (2012).
10. L. M. Robeson, *J. Membr. Sci.* **320**, 390–400 (2008).
11. H. Suda, K. Haraya, *J. Phys. Chem. B* **101**, 3988–3994 (1997).
12. P. Y. Huang *et al.*, *Nature* **469**, 389–392 (2011).
13. D. L. Duong *et al.*, *Nature* **490**, 235–239 (2012).
14. C. H. Lui, L. Liu, K. F. Mak, G. W. Flynn, T. F. Heinz, *Nature* **462**, 339–341 (2009).
15. D. A. Dikin *et al.*, *Nature* **448**, 457–460 (2007).
16. Y. W. Zhu *et al.*, *Adv. Mater.* **22**, 3906–3924 (2010).
17. R. R. Nair, H. A. Wu, P. N. Jayaram, I. V. Grigorieva, A. K. Geim, *Science* **335**, 442–444 (2012).
18. M. S. Spector, E. Naranjo, S. Chiruvolu, J. A. Zasadzinski, *Phys. Rev. Lett.* **73**, 2867–2870 (1994).
19. S. K. Bhatia, M. R. Bonilla, D. Nicholson, *Phys. Chem. Chem. Phys.* **13**, 15350–15383 (2011).

20. L. J. Cote, F. Kim, J. X. Huang, *J. Am. Chem. Soc.* **131**, 1043–1049 (2009).
21. A. Torrisi, C. Mellot-Draznieks, R. G. Bell, *J. Chem. Phys.* **132**, 044705 (2010).
22. M. B. Rao, S. Sircar, *J. Membr. Sci.* **85**, 253–264 (1993).
23. H. B. Park *et al*., *Science* **318**, 254–258 (2007).
24. I. Pinnau, W. J. Koros, *Ind. Eng. Chem. Res.* **30**, 1837–1840 (1991).
25. N. Y. Du *et al*., *Nat. Mater.* **10**, 372–375 (2011).
26. D. Shekhawat, D. R. Luebke, H. W. Pennline, "A review of carbon dioxide selective membranes: A topical report" (Report DOE/NETL 2003/1200, U.S. Department of Energy, National Energy Technology Laboratory, Pittsburgh, PA, 2003).
27. J. C. Poshusta, R. D. Noble, J. L. Falconer, *J. Membr. Sci.* **186**, 25–40 (2001).
28. S. Eigler, C. Dotzer, A. Hirsch, M. Enzelberger, P. Muller, *Chem. Mater.* **24**, 1276–1282 (2012).
29. M. B. Shiflett, H. C. Foley, *Science* **285**, 1902–1905 (1999).
30. R. M. de Vos, H. Verweij, *Science* **279**, 1710–1711 (1998).

Acknowledgments: This work was mainly supported by Korea Carbon Capture and Sequestration Research and Development Center (KCRC) (grant no. 2012-0008907) funded by the Korea government (Ministry of Science, Information Communication Technology and Future Planning). We thank the National Synchrotron Light Source at Brookhaven National Laboratory for providing the X9 beam line (grant no. DE-AC02-98CH10886) and B. D. McCloskey for thoughtful reading and commentary on our paper. H.B.P. also acknowledges support by the research fund of Hanyang University (grant no. 200900000001052).

Supplementary Materials
www.sciencemag.org/content/342/6154/91/suppl/DC1
Materials and Methods
Figs. S1 to S10
References (*31*, *32*)

4 February 2013; accepted 4 September 2013
10.1126/science.1236098

Ultrathin, Molecular-Sieving Graphene Oxide Membranes for Selective Hydrogen Separation

Hang Li,[1,2] Zhuonan Song,[1,2] Xiaojie Zhang,[1,2] Yi Huang,[1,2] Shiguang Li,[3] Yating Mao,[1] Harry J. Ploehn,[1] Yu Bao,[4] Miao Yu[1,2]*

Ultrathin, molecular-sieving membranes have great potential to realize high-flux, high-selectivity mixture separation at low energy cost. Current microporous membranes [pore size < 1 nanometer (nm)], however, are usually relatively thick. With the use of current membrane materials and techniques, it is difficult to prepare microporous membranes thinner than 20 nm without introducing extra defects. Here, we report ultrathin graphene oxide (GO) membranes, with thickness approaching 1.8 nm, prepared by a facile filtration process. These membranes showed mixture separation selectivities as high as 3400 and 900 for H_2/CO_2 and H_2/N_2 mixtures, respectively, through selective structural defects on GO.

Zeolites (*1*, *2*), silica (*3*), carbon (*4*), and polymers (*5*) have been made into microporous membranes that have shown promising gas mixture separation performance. These membranes separate mixtures on the basis of selective adsorption, diffusion rate differences, or molecular-sieving mechanisms. Current microporous membranes, however, are usually thicker than 20 nm to minimize undesirable flux contribution through nonselective membrane defects, and they maintain reasonably high separation selectivity.

Graphene-based materials, such as graphene and graphene oxide (GO), have been considered promising membrane materials, because they are only one carbon atom thick and, thus, may form separation membranes that minimize transport resistance and maximize flux. Additionally, they have good stability (*6*, *7*) and are mechanically strong (*8*). Graphene-based materials have been made into centimeter-sized, thick (~1-μm) membranes and micrometer-sized, isolated single sheets for pure component permeation studies where they were found to be either impermeable to small gas molecules or not practical for separation applications (*9*–*12*).

We used single-layered GO flakes, prepared by the modified Hummer's method (*13*). Ultrathin GO membranes were prepared by vacuum filtration, as described in detail in fig. S1. Centrifugation and dilution of GO dispersions were found to be important for preparing high-quality GO membranes [fig. S2 and discussion in (*13*)]. Figure 1A shows a ~9-nm-thick GO membrane with a permeation area of ~4 cm^2 on anodic aluminum oxide (AAO) support. A glass membrane module was used for gas permeation-separation experiments, as shown schematically in fig. S3. X-ray diffraction shows the characteristic peak of GO at 2θ of 11.1° [fig. S4 and analysis in (*13*)], and GO flakes are ~500 nm in size and single-layered, as confirmed by atomic force microscopy (AFM) (Fig. 1B), which also shows the height profile of a GO flake (Fig. 1C). In Fig. 1, panels D and E show the surface of an 18-nm-thick GO membrane on AAO. Compared with the AAO support (Fig. 1F), a very thin GO coating can be seen. We deposited a relatively thick GO membrane [~180 nm (Fig. 1G)] to correlate the GO deposition with the membrane thickness. GO dispersion for this 180-nm–membrane preparation was then diluted 100, 20, and 10 times to obtain the above 1.8-, 9-, and 18-nm-thick GO membranes, respectively, assuming no GO loss during filtration and constant membrane density. We used x-ray photoelectron spectroscopy (XPS) to detect surface elements for these ultrathin GO membranes on AAO (Fig. 1, H and I). For a 1.8-nm-thick membrane, a substantial amount of aluminum can be seen, because the mean free path of excited electrons is longer than the surface GO membrane thickness. However, for thicker membranes (9 and 18 nm), much smaller amounts of the underlying aluminum can be seen, because GO thickness is larger than the excited electron mean free path. This finding is consistent with surface carbon detection by XPS as well (Fig. 1I). See the supplementary materials for a detailed analysis.

We conducted permeation tests with different light gas molecules to probe pore sizes. Hydrogen (kinetic diameter: 0.289 nm) permeated ~300 times faster than did CO_2 (0.33 nm) through a ~18-nm-thick GO membrane at 20°C (Fig. 2A). Their kinetic diameter difference is only 0.04 nm, suggesting that the average size of pores for permeation in the GO membrane may be between 0.289 and 0.33 nm. O_2 and N_2 showed similar permeance as CO_2. However, CO and CH_4 had slightly higher permeance, although these molecules are are slightly larger than the aforementioned ones. Koenig *et al*. (*12*) also found that CH_4 had slightly higher permeance than N_2 through pristine graphene flakes, though the reason is still unclear. Figure 2B shows H_2 and He permeances for GO membranes with different thicknesses. Gas permeance is usually inversely proportional to the membrane thickness for conventional membranes (*14*). Surprisingly, we found that H_2 and He permeances decrease exponentially as membrane thickness increases from 1.8 to 180 nm (Fig. 2B). We speculate that the major transport pathway for these molecules is selective structural defects within GO flakes, instead of spacing between GO flakes. Reduction has been shown as an effective way to narrow interlayer spacing in GO membranes and, thus, limit permeation of molecules through spacing (*10*). We reduced GO membranes with thickness from 1.8 to 20 nm and conducted pressure-driven water permeat ion. We found that water permeance decreased approximately three orders of magnitude: For example, water permeance through a 3-nm GO membranes was 1370 liters/(m^2·hour·bar), whereas it was 0.5 to 1 liters/(m^2·hour·bar) through

[1]Department of Chemical Engineering, University of South Carolina, Columbia, SC 29208, USA. [2]Catalysis for Renewable Fuels Center, University of South Carolina, Columbia, SC 29208, USA. [3]Gas Technology Institute, 1700 South Mount Prospect Road, Des Plaines, IL 60018, USA. [4]College of Applied Science and Technology, Rochester Institute of Technology, Rochester, NY 14623, USA.

*Corresponding author. E-mail: yumiao@cec.sc.edu